Prospects of High Precision Fiber for Gravitational Wave Detection

Danial Shadmany

shadmany@stanford.edu

Submitted in partial satisfaction of the requirements for the degree of

BSc (Hons) Physics

Department of Physics

Stanford University

2020

Abstract

All current gravitational wave (GW) detectors, such as those of the Laser Interferometer Gravitational-wave Observatory (LIGO) and Virgo, are precision optical interferometers with sub-attometer displacement sensitivity. Free space propagation of the optical beams of LIGO requires large (meter diameter and kilometers of length) evacuated stainless steel beam tubes that come with sizable manufacturing and operational costs. A fiber based detector – with the free space beams of present schemes replaced by concentrated fiber spools – could mitigate these costs while simultaneously offering a more compact experimental setup. But whether fiber technologies can achieve the noise sensitivity required to detect GWs is still an open experimental question.

Optical fiber technology was first examined as a candidate platform for GW detection in the late 1980s. Since then, much progress has been made in modeling and reducing noise sources in single-mode silica-based fibers. Additionally, the development of novel fiber technologies, e.g. hollow core and photonic crystal fibers, have generated excitement for improved noise profiles when it comes to thermal delay constants and scattering sources. To our knowledge no comprehensive recent reassessment of the noise properties of optical fibers aimed at gravitational wave detection exists in the literature.

Here we carry out calculations of the strain sensitivity for a hypothetical Michelson interferometer with silica-based fibers in each arm. Limits to sensitivity arising from thermoconductive, thermomechanical, and shot noise sources are established and compounded to arrive at an estimate of the overall noise floor. Considering an interferometer with kilometers of arm length, comparable to that used in the cur-

rent generation of GW detectors, we estimate the strain at 100 Hz to be around $10^{-16}\sqrt{Hz}$. This is a factor of a million worse than what has been achieved by Advanced LIGO. While sobering, avenues exist which might lead to gains in sensitivity. Advanced cooling strategies, novel fiber technologies, and parameter tuning in the thermal noise model all have the potential to drive improvements. We conclude by summarizing the major developments in each area.

Acknowledgements

Thank you, first of all, to Nergis. Not only for giving me the opportunity to work in her lab during COVID, but also for being an astounding role model, for investing in my future as a scientist, and for creating an incredibly positive and motivating atmosphere in which to do work. Working at MIT LIGO is a real privilege.

I'd also like to thank Vivishek Sudhir, Benjamin Lane, Haocun Yu, Alvaro Fernandez, Matt Evans, Lee McCuller, and everyone at MIT LIGO for programming help, late night Slack conversations, and general guidance. Thank you to Ben in particular for introducing me to MIT LIGO last summer and for being a terrific summer research graduate mentor. Big thanks to Vivishek as well for his many comments and insights - too many for a cataloguing - on numerous projects over the past year.

Philip Walther and Christopher Hilweg at the University of Vienna have been amazing collaborators. Thank you to Chris for comments on the design of the fiber interferometer, for the contribution of the Faraday mirrors, and for his comprehensive knowledge of noise sources in fibers. I'm excited to see where our collaboration goes.

Thank you to Pat Burchat for being an amazing source of advice and support over the past four years and for recommending that I reach out to/work with Nergis in the first place. Thank you to Peter Graham for teaching me general relativity and for serving as the second reader on this project.

Finally, thank you to my family and friends, without whom this thesis would not have been possible.

Hannah, Harris, Mom, Dad - I love you all.

Table of Contents

1 Introduction **1**

1.1 Free Space Propagation in LIGO: Theory and Design 5

1.2 Proposed Design for a Fiber Interferometer 8

2 Thermal Noise **11**

2.1 The Fluctuation Dissipation Theorem 12

2.2 Thermoconductive Noise 16

2.3 Thermomechanical Noise 22

3 Scattering Noise Sources **25**

3.1 Stimulated Brillouin Scattering 25

3.1.1 Solution for the Density Variation and Power Threshold . . . 26

3.2 Stimulated Raman Scattering 29

4 Results **30**

4.1 Thermal Noise 30

4.2 Shot Noise 33

4.3 Brownian Noise and Fiber Amplifiers 34

5 Conclusion and Future Directions **35**

List of Figures

1.1 LIGO strain sensitivity curve in September 2015, at the time of the first detection of gravitational waves [1] 2
1.2 Diagram of a Michelson Morley Interferometer with 3 km arm length, including beam splitter and output photodetector [9] 5
1.3 Simple image depicting constructive and destructive interference. [22] 6
1.4 Classic schematic of a confocal Fabry-Perot cavity [8] 7
1.5 Proposed geometry for a Michelson "fiber interferometer." 9

2.1 Gaussian beam profile of light propagating in fiber [6] 20

3.1 Dispersion diagram showcasing the input and output momenta/energy of the particles involved in SBS [13] 26

4.1 Thermomechanical (blue, green), and thermoconductive (red) noise curves for an interferometer arm length of 10 km at room temperature. 31
4.2 Shot noise comparison between 60 mW light beam propagating in fiber (blue) and Advanced LIGO operational power of about 33 W (red). Power level in fiber set to minimize SBS and SRS effects. 32
4.3 Strain sensitivity of total thermal-optic (purple) and thermo-mechanical (blue) noise sources in fiber plotted in reference to the Advanced LIGO sensitivity curve 32

Chapter 1

Introduction

In any precision measurement, one of the most important factors is the noise sources that limit our ability to measure the desired signal – the signal-to-noise ratio (SNR). Gravitational wave detection – observing perturbations in the very fabric of space-time arising from violent cosmic events – requires measuring changes in spacetime distances smaller than attometers. Seismic, thermal, quantum shot, and a whole potpourri of environmental noises limit the sensitivity of gravitational wave (GW) detectors. In 2015, the decades-long efforts by LIGO scientists towards isolating and mitigating such minuscule yet limiting effects paid off in grand fashion with the first direct detection of gravitational waves [1].

The signal involved in that measurement - an astronomical chirp representing the collision of two black holes 1.3 billion light years away - was read out against a background of noise sources that are given by the sensitivity curve shown in Fig 1 below. This plot represents the detection capability of the Advanced LIGO instrument, the smallest perturbations in "GW strain" [1] that LIGO is able to resolve. In the sections below, we will expand on how lowering this strain sensitivity is deeply related to detecting the changes in spacetime caused by a passing GW. But suffice it to say that over the past two decades a large scientific community has been devoted to improving the strain sensitivity of LIGO, lowering the "noise" component of a signal-to-noise ratio.

[1] GWs cause changes in distance proportional to the distance itself, a strain. Converting between strain and displacement is a matter of multiplying displacement by the length of the detector, or 4000 m in the case of LIGO.

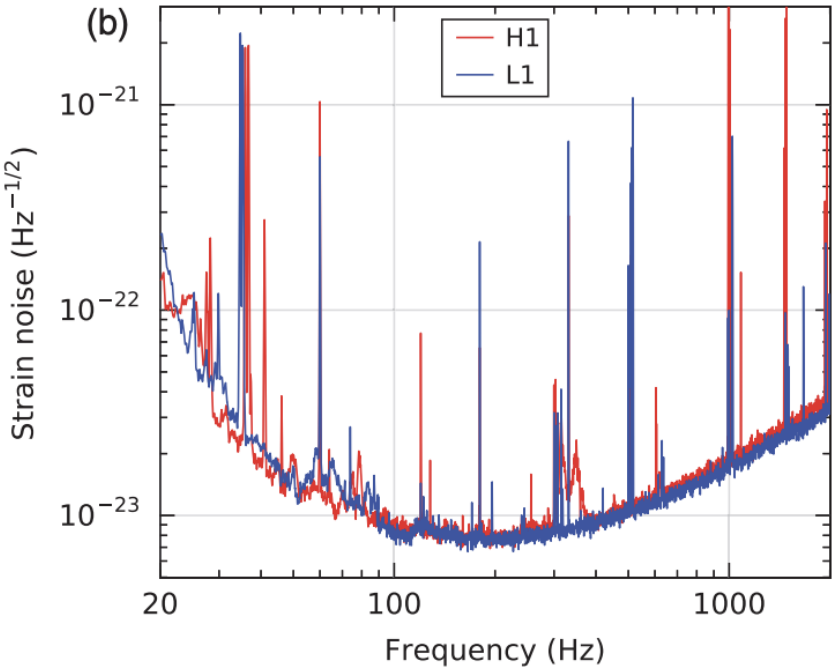

Figure 1.1: LIGO strain sensitivity curve in September 2015, at the time of the first detection of gravitational waves [1]

The effect of GWs we are trying to observe with LIGO is infinitesimally small. In order to confidently distinguish between a GW and random background fluctuations, the SNR needs to be as large as possible. Above, we stated that the strain sensitivity curve represented the noise component of a signal-to-noise ratio. Within the body of this thesis, **noise refers to uncertainties arising from fluctuations of the measuring system**. Some fluctuations, such as vibrational or thermal noise, can be mitigated by better engineering of isolation systems, material or geometric properties. Others, such as quantum shot noise, are more fundamental and require clever quantum sensing schemes such as injection of squeezed states of light [Ref]. It will also be useful to pin down what we mean by a signal to noise ratio: the signal-to-noise ratio is **a measure of the strength of some information carrying signal of interest versus the background interference against which the signal is measured**. It follows that if the background interference is too strong, the signal is immeasurable; nothing is detected.

Achieving high SNR in LIGO requires an enormous investment of resources. One of

the largest cost drivers in LIGO are the beam tubes maintained at ultrahigh vacuum conditions, needed for free-space propagation of the optical beams currently used. The engineering design challenges, the cost, and the need for large tracts of land that are typically sited in remote locations all motivate the search for alternative, more compact, and potentially cheaper solutions with comparable sensitivity.

One option is the use of optical fiber technology. The prospect of a fiber-based GW detector has persisted as a nascent possibility. It presents a road to a coiled setup where the long interferometer arms of current schemes are replaced with "fiber spools," guiding in the light in a constricted space through many round trips. Such a setup would allow for compact operation from laboratories and could save on some of the costs and complexity of major observatories.

Fiber interferometry was first considered as an option during the late 1980's in the original Bluebook for LIGO [16]. At that point, Brillouin and Raman scattering noise sources were shown to impose a fundamental and crippling limit on input power and thus on shot noise limited performance [2]. Combined with the stringent thermal noise profile of fibers, the idea of a fiber-based interferometer seemed impractical at that time.

Since then, much progress has been made in modeling and reducing noise sources in single-mode Silica-based fibers. Additionally, the development of novel fiber technologies, e.g. hollow core and photonic crystal fibers, have generated excitement for improved noise performance when it comes to thermal delay constants and scattering sources. While the outlook is still difficult, our understanding of and ability to mitigate noise in fibers has advanced, but to our knowledge no comprehensive reassessment of the noise properties of optical fibers aimed at gravitational wave detection exists in the literature.

Given the advances in optical fiber technology since the 1980s, the purpose of this

[2]Since shot noise scales as the square root of laser power in an optical measurement, the SNR of the measurement improves with larger power. Nonlinear effects, however, dominate the noise performance of optical fibers with high laser powers, which sets a limit on the lowest shot noise achievable.

work is to revisit the possibility using optical fibers for GW detection. We carry out calculations of the strain sensitivity for a hypothetical Michelson interferometer with silica-based fibers in each arm. Limits to sensitivity arising from thermoconductive, thermomechanical, and shot noise sources are established and compounded to arrive at an estimate of the overall noise floor.

Section 1.1 begins with an overview of the current free-space beam setup in LIGO. After describing the general layout, cavity design, and theory behind the free-space beam detector, we propose an analogous setup with compact fibers. In order to achieve the long arm length required for a GW detector, we spool the fiber length around many times in an elliptical shape, equivalent to propagating the light through multiple round trips. A more detailed description of our design can be found in Section 1.2.

Subsequently, we carry out the strain sensitivity calculations for the fiberoptic setup. Chapter 2 develops the Wanser and Duan theories of thermal noise, the most pronounced limitation on the fiber noise floor and consequently on the signal to noise ratio. The Fluctuation-Dissipation theorem is a general framework for examining such thermal noise sources and can be used to link equilibrium fluctuations with the dissipative properties of a system. Section 2.1 lays out this theory in its general form, while Sections 2.2 and 2.3 apply it to the two classes of thermal noise which most seriously afflict fibers: thermoconductive and thermomechanical sources.

Scattering noise sets another intrinsic limitation on the SNR of precision fiber interferometry. However, the influence of scattering noise (typified by Brillouin and Raman scattering sources) is more subtle. The thermal noise sources described above serve as fundamental limits on strain. The scattering sources, by contrast, serve as fundamental limits on *power*. The importance of achieving high powers will be immediately apparent to specialists in quantum detection: the higher the power, the lower the shot noise limited sensitivity. Chapter 3 will examine this dynamic.

Chapter 4 briefly examines other noise sources and complicating factors, including attenuation in fibers and amplifier noise. Section 4.2 pulls it all together: combining

the calculations from the thermal and scattering theories in order to arrive at an overall sensitivity curve for noise in fiber.

Having characterized the limits of fiber interferometry, Chapter 5 puts it all in context. While the strain sensitivity achievable in state-of-the-art Silica fibers is many orders of magnitude away from achieving the requisite performance for detecting GWs, this thesis concludes by summarizing the path to improvement, including advanced cooling schemes and the possibility of enhanced noise mitigation in photonic crystal and/or hollow core fibers.

1.1 Free Space Propagation in LIGO: Theory and Design

LIGO can be viewed as a kind of transducer: it takes a difficult to measure infinitesimal perturbation in length (spacetime), and converts it into something more amenable to scientific analysis, a signal in the audioband that can be registered on a photodetector.

The instrument of choice for such transduction is a Michelson interferometer, consisting of two orthogonal "arms" within which laser light circulates. The interferometer is designed for detecting subtle differences in the path length traversed by the light in one arm relative to the other arm.

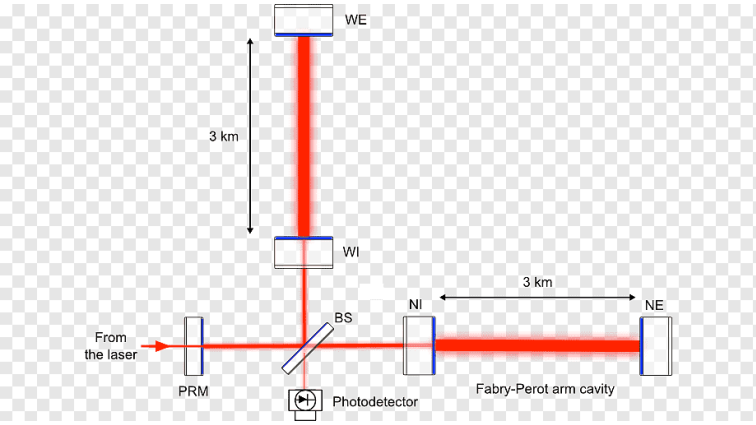

Figure 1.2: Diagram of a Michelson Morley Interferometer with 3 km arm length, including beam splitter and output photodetector [9]

Laser light is an exquisite tool for registering such minute changes. The oscillations of light - its phase - can be thought of as both accurate timekeeper and ruler. By controlling as much as possible for differences in path length between the two arms, the two light beams can be made to remain *in phase* for the duration of the transit time. Consider a laser beam incident on the beam splitter (BS) depicted in Figure 1.2. The emergent rays diverge perpendicularly, each directed into a cavity arm of length 4 km. After reflecting off of the cavity back mirror, the rays eventually exit the cavities through the same port they entered, interfering with each other on the back end of the BS to create a signal on the photodetector.

If the two arms are carefully configured to the exact same effective path length (modulo fluctuations which can be controlled for using a translatable mirror or other actuation), the light will interfere constructively. The signal on the photodetector will be maximal. Conversely, if the two arm lengths are not so perfectly identical, differences or *noise fluctuations* between the two arms might be large enough to break such constructive interference, introducing a phase misalignment and leading to a reduced signal amplitude on the output. In essence, we have taken something that is difficult to measure, the slightest differences in length between two arms, and converted it into changes in laser power, a powerful and productive tool in experimental physics.

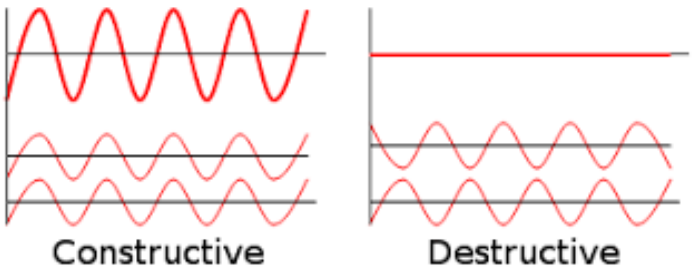

Figure 1.3: Simple image depicting constructive and destructive interference. [22]

This sensitivity of signal amplitude to phase difference is actually a *good thing*. Indeed, the passing of a GW itself manifests as a contraction of length in one direction and an expansion of it in another. One arm length is stretched, while the other is

compressed, resulting in a variation in effective path length between the two arms. Such a variation is so infinitesimally small so as to be imperceptible to other schemes for detecting changes in length, washed out by background noise. But the circulation of light in a Michelson interferometer provides a unique platform where careful engineering and control can create conditions optimized for detection of tiny GW-induced displacements of the mirrors of the interferometer.

The description above has left out two important points. First, is the scaling of detection sensitivity with arm length. Strain sensitivity in LIGO is calculated by taking the displacement (or phase) noise caused by some source (e.g. thermal) and dividing it by the total length (or equivalent phase shift) of the detector L. However, it is important not to make generalizations as to the linear scaling of detector sensitivity with length, since each noise source tends to have a different scaling with L [7]. As a general rule however, the larger the arm length L, the more sensitive is LIGO to non-background effects such as a gravitational wave. The current generation of Advanced LIGO detectors employ interferometers with 4 km long arm lengths.

The second important point has been foreshadowed above: the *circulation* of light within the interferometer arms. From Figure 1.2, it might be easy to suppose that the outgoing light rays from the BS only take one round trip through the interferometer arms, bouncing a single time off of the back mirror before returning to the initial BS. Instead, light in each arm enters a Fabry-Perot cavity, bouncing back and forth a few 100 times between the input and end mirrors, before eventually leaking back

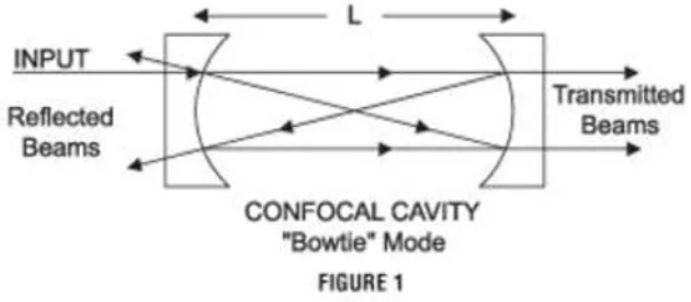

Figure 1.4: Classic schematic of a confocal Fabry-Perot cavity [8]

out. This circulation of light serves two purposes. First, it builds up laser power within the cavity, leading to an overall circulating power of 750 kW, essential for attaining the requisite sensitivity for detecting GWs. Second, it extends the effective length of the interferometer arm to over 1000 km. The number of round trips the light makes is arranged by the transmissivity and reflectivity of the mirrors.

These points about the scaling of detection sensitivity which length and the circulation of light in the LIGO arms will become important as we consider designs for fiber detectors. In subsequent sections, we will face the dual problems of how to realize longer arm lengths in fibers, where thermal noise and attenuation effects increase with L in a way not present in LIGO, and also of how to recreate the circulation and build up of power that the arm cavities provide for LIGO.

1.2 Proposed Design for a Fiber Interferometer

The prime benefit of a fiber-based GW detector is the possibility of a more compact experimental setup. Here, we describe a proposed design for this compact fiber interferometer, manifesting as a Michelson interferometer where the arm cavities are replaced by wound fiber spools, carrying the light through many round trips. In imagining our experimental setup, we have chosen to "dream big," envisioning that the technical problems involved in spooling tens of km of fiber in a compact space can be solved with creative engineering. Before investing the enormous effort involved in realizing such a setup, it would be good to know whether it is worth realizing in the first place. For this reason, we chose to focus on fundamental noise limitations rather than engineering ones for the preliminary investigations of this thesis.

Fig 1.4 depicts our proposed interferometer design. Just as the schematic for the traditional Michelson interferometer shown in Fig 1.2, a laser beam is incident on a BS. Unlike the classical setup, however, the beams past the BS do not enter a cavity within which they circulate back and forth. Instead, the beams are mode matched to launch into a fiber spool, where the light accumulates an effective arm length of, say, 10 km (the number of windings required to amass 10 km in a compact setup might

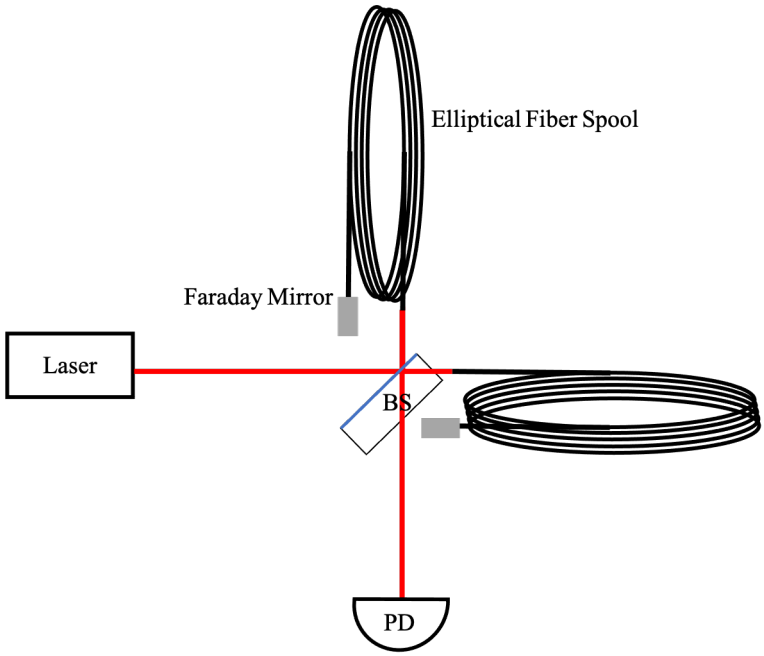

Figure 1.5: Proposed geometry for a Michelson "fiber interferometer."

seem intimidating, but it is our hope that clever tricks could be used to for example distribute the number of windings across multiple spools, etc). After passing through the spool and reflecting off the end mirror, the light exits through the same input, interfering with the its counterpart from the orthogonal arm spool, and creating an output signal on the photodetector in a similar manner to the original Michelson scheme.

One concern not present for free-space beam interferometers, but at issue for fibers, is maintaining the polarization of the circulating light. Light traveling in a single-mode fiber can experience random fluctuations in polarization induced by stress, vibration, and temperature changes. To combat this issue, we propose that the end reflection be accomplished by a so-called "Faraday mirror," which both reflects the light and rotates its polarization by 90°. This has the effect of canceling out any variations in polarization that might have been introduced during the transit time, while simultaneously serving allowing the light to travel backwards through the fiber without interfering with the forward propagating beam.

Polarization effects, however, are not the only sources of noise in fibers. As mentioned

in the introduction, a whole potpourri of effects contribute to optical losses and noise in fibers. Thermal noise, scattering, and other processes unique to fiber must be considered to guide the realization of such a detector for measuring GWs. Having laid out the overall design of our setup, we now examine its capabilities in the subsequent sections, exploring the specific models and calculations which set limitations on the strain sensitivity of our proposed fiber interferometer.

Chapter 2

Thermal Noise

Thermal noise sources are the largest impediment to achieving the sensitivity needed for detecting GWs with fiber interferometers, setting an essential limit on the strain sensitivity, and hence the SNR that can be achieved in such systems. In this section, we conduct a general review and derivation of the most punishing sources of thermal noise and their consequences for detecting GWs.

The overwhelming proportion of intrinsic thermal noise in fibers can be attributed to thermoconductive and thermomechanical effects [2, 6, 21]

- Thermoconductive effects result from fluctuations in temperature, which drives thermal expansion and variations in the temperature-dependent refractive index of the fiber.
- Thermomechanical effects are associated with random expansion or contraction of the fiber caused by internal friction (i.e. structural damping).

These effects have been extensively studied by Wanser, Foster, Duan, and others [2, 6, 21].

In a 2013 paper [6], Duan made a key contribution by demonstrating that both thermomechanical and thermoconductive effects could be derived under the simple framework of the fluctuation dissipation theorem (FDT)[3]. A wide ranging concept with large implications, we devote the first part of this section to developing the

FDT with an eye towards employing it to derive expressions for the thermal noise profiles of interest.

2.1 The Fluctuation Dissipation Theorem

Equilibrium dynamics form the bulk of most introductory courses in thermodynamics. Typically, such processes are reversible and can be understood using variants of the First Law of Thermodynamics with a chemical potential term. However, when thinking about processes which include dissipation, loss, and noise (such as occurs for light propagating in a fiber) a different development is needed. For non-equilibrium, irreversible, or dissipative phenomena our tool set is much more limited.

The Fluctuation-Dissipation theorem (FDT) is a powerful idea [3, 14]. It relates a system's equilibrium fluctuations to the non-equilibrium response of that same system to external forces. In 1905, Einstein discovered the most famous instance of the theorem [14]. Consider the Brownian motion of particles. For specificity's sake, we consider the instance of colloidal particles floating in a liquid medium. When observed under a microscope, one perceives the random vibrations of such particles, a phenomena which arises due to impacts with the liquid molecules. Even in thermal equilibrium these fluctuations – labeled Brownian motion – are manifest.

Now consider a very different and seemingly unrelated effect. Suppose an external force is applied to the system. For the charged particles above, an applied electric field gives rise to two effects: on the one hand, the particles are directed through the medium as described by Lorentz's force law; on the other hand, random collisions with the liquid resist this motion, giving rise to a frictional force.

The insight at the heart of FDT is that because equilibrium Brownian motion and non-equilibrium frictional effects have the same origin - i.e. random collisions with the background medium - they can be tied together mathematically. Concretely, the generalized fluctuations can be expressed in the frequency domain as a power spectral density. The response of a general system to an external force can be characterized

to first order by the admittance $Y(\omega)$, and dissipation is represented in part by the real part of Y.

The FDT then relates fluctuation and dissipation as follows:

$$S_x = \frac{k_B T}{\pi \omega^2} ReY(\omega). \tag{2.1}$$

What we have then is a general procedure for determining the noise profile of some arbitrary parameter x given an understanding of the admittance function which quantifies the system's response to external forces. Since it is, as a general rule, much easier to calculate $Y(\omega)$ – thermomechanical noise, for example, can be examined using the normal mode expansion, where the admittance function $Y(\omega)$ simply becomes a sum over a set of harmonic oscillators with damping. This is a powerful result.

Deriving equation (2.1) requires a more sophisticated mathematical apparatus than we have going here. However, it would be instructive to gain intuition as to how exactly fluctuation and dissipation come to be related. Einstein anticipated the FDT when he noticed that the viscous friction of a particle undergoing Brownian motion is related to its diffusion constant by the following expression:

$$D = \frac{k_B T}{m_\gamma}, \tag{2.2}$$

which accords with our intuition that lower friction should lead to greater diffusivity. Here, $m_\gamma = \frac{1}{\mu}$, where μ is defined as the mobility, or the drift velocity of particles at a given value for the electric field.

Diffusivity itself, however, can be related to the equilibrium fluctuations for the velocity of a particle undergoing Brownian motion. To see this, we begin with the following expression for diffusivity:

$$D = \lim_{t \to \infty} \frac{1}{2t} \left\langle \{x(t) - x(0)\}^2 \right\rangle . \tag{2.3}$$

This expression might seem strange, but it becomes intuitive once one recalls that (i) that the expectation of Δx^2 is akin to the standard deviation of a random walk after n steps, which is not zero, and that (ii) the time term in the denominator serves as normalization. This expression serves to capture net fluctuations in distance over time for a particle in a medium, in keeping with one's intuitive sense of the diffusion constant D.

However, the quantity $x(t) - x(0)$ can be written as the integral over velocity. Substituting into the square and bringing the expectation value into the integral:

$$D = \lim_{t \to \infty} \frac{1}{2t} \int_0^t dt_1 \int_0^t dt_2 \;\; u(t_1)u(t_2) \;\; . \tag{2.4}$$

A clever substitution for u, followed by an evaluation of the limit can be shown to yield [14]:

$$D = \int_0^\infty \;\; u(t_0)u(t_0 + t) \;\; dt \tag{2.5}$$

This is an expression for diffusivity in terms of the fluctuations of the velocity of the particle's velocity. Substituting our the alternative expression for diffusivity, stated above in Eq 2.2, we arrive at:

$$\mu = \frac{1}{m_\gamma} = \frac{1}{k_B T} \int_0^\infty \;\; u(t_0)u(t_0 + t) \;\; dt, \tag{2.6}$$

where the inverse of the friction constant is known as the mobility. Let us recap what we have just shown. We started from two expressions for diffusion, one as related to the friction constant (Eq. 2.2), and the other as related to expected value of distance traveled. By manipulating the second, we were able to tie diffusion to

expected fluctuations in the velocity of the Brownian motion. Finally, we came full circle and connected the equilibrium fluctuations of the particle to its overall mobility, or friction.

This is a powerful procedure, which depends on the idea that the frictional force an object experiences in a medium when an external force is applied to it (its mobility) can be related to the variance arising from random Brownian fluctuations of an object that is dropped into the medium with no external forces. Consider the following two situations: (1) where a particle is dropped into a fluid and then an external field is applied to it so that it experiences motion in some direction, and (2) the particle is dropped into the fluid, except with the field turned off. In the first case, it is clear the object moves, in the direction of the applied field. In the second case, the particle also moves, but very differently: it jiggles randomly due to Brownian motion. In the first case, we expect the particle to accumulate net distance over time. In the second case, the particle's position fluctuates, but the net distance accumulated is zero.

It is difficult to relate these effects because in one case there is net motion and the other there is not. However, the fluctuation dissipation theorem subverts this problem by drawing our attention to something else. The first lesson from the random walk is that while the mean over n steps is 0, the standard deviation scales with the $\sqrt{n}$. Likening the motion a particle experiences during Brownian motion to a random walk, the particle which has been dropped into our fluid undergoes no net motion, but over time its variance grows larger and larger. The rate at which this variance grows is a property of the fluid, a consequence of the way in which randomly fluctuating particles interact with each other. Equation 2.2 takes this variance and divides by time to normalize it. Then, instead of comparing net distance, the fluctuation-dissipation theorem compares the normalized variance of an equilibrium particle with the frictional properties of the medium. In essence, an equivalence is drawn between the ease with which the probability distribution of a particle in equilibrium spreads itself out (while maintaining a constant mean) and the propensity of that medium to resist changes to non-equilibrium forces.

The hope is that the preceding exercise has provided intuition as to the power and general applicability of the fluctuation-dissipation theorem. Returning to the more precise statement of the theorem above:

$$S_x = \frac{k_B T}{\pi \omega^2} ReY(\omega), \tag{2.7}$$

we see again the fluctuations on the right hand side (captured using a power spectral density) equated to the linear response to external force, or admittance, on the left. This idea is an essential tool for non-equilibrium thermodynamics. In the coming sections, we will use it to take something which is easy to calculate for fibers (power dissipation) and convert into the thermal phase noise spectra which we are interested in investigating for our interferometers.

2.2 Thermoconductive Noise

The above treatment of the fluctuation dissipation theorem might have ended on a dissatisfying note: in connecting the example of Brownian motion with the expression for power spectral density in terms of admittance (equation (2.7)), we made a loose leap from a specific and simplified example to a much more involved equation. While fully teasing out the relationship between the two cases would involve examining the full proof of the FDT, the reader still might have lingering practical concerns: how does one actually apply such an equation towards deriving noise in an actual physical system, a fiber interferometer, for example. In this section, we go through the specific example for thermoconductive noise in fiber.

Thermoconductive noise arises due to temperature fluctuations in fiber. Such fluctuations manifest as phase noise in two ways. First, through the corresponding expansion and contraction of the fibers, and second through variations in the temperature-dependent index of refraction. By changing the length of the interferometer arms, expansion and contraction cause variations in the phase of the circulating light, introducing a path length difference between the two arms with the potential to

overshadow the phase signal of a passing GW. Variations of the index of refraction also introduce a path length difference, though by a different mechanism: by causing changes in the ***speed*** of the light, the light is made to arrive at a different point in time than it otherwise might have, leading to a difference in the interference signal at the output.

From the discussion above it should be apparent that the word "phase noise" is a really a stand in for mechanisms that might influence (a) the actual length of the path that the light travels, (b) the speed of traveling light, or (c) the time light takes to travel. Such parameters are linked together and impact phase, and the "equivalence" between a phase difference and length/time difference is useful for gaining intuition for these systems.

For thermal noise sources, then, there are two means by which temperature fluctuations manifest as phase noise. In order to derive a general expression for the power spectral density of this phase noise, we will need two things: (1) an expression for phase fluctuations in terms of temperature fluctuations, and (2) a subsequent expression for temperature fluctuations in terms of the parameters of the fiber.

The first expression is provided by Foster et. al [10]. The two effects can be accounted for simultaneously as a factor multiplied onto the power spectral density (PSD) for temperature fluctuations.

$$S_\phi = \frac{4\pi^2 l^2}{\lambda^2}\left(\frac{dn}{dT} + n\alpha_L\right)^2 S_{\delta T}(\omega) \tag{2.8}$$

where S_ϕ stands for the PSD of thermoconductive phase noise, $S_{\delta T}$ for the PSD of the temperature fluctuations, and where ω, λ, T, and n correspond to angular frequency, laser wavelength, temperature, and index of fraction, l to the length of the fiber, and α_L to the thermal expansion coefficient. Within the parenthesis, the left hand term captures the changes in refractive index, while the right hand term the variations in fiber length due to thermal expansion and contraction.

The expression above, however, leaves the fluctuations in temperature unspecified. In

order to work with S_ϕ, we will need an equation for $S_{\delta T}$. This is where the fluctuation dissipation theorem comes in. By giving us a procedure for mapping something which is relatively easy to derive (dissipative effects) to something which is more difficult (temperature fluctuations), we can use "test forces" to understand the dissipative properties of our model and from there work to solve for thermoconductive noise in fibers.

The procedure we follow for this derivation was developed by Levin for understanding the intrinsic thermal noise properties of the LIGO test masses [15], and can be applied to thermoconduction in the following manner. Beginning with the statement of the fluctuation dissipation theorem from the previous section:

$$S_x = \frac{k_B T}{\pi \omega^2} ReY(\omega), \tag{2.9}$$

where the parameter x is a general stand in for the fluctuating variable of the system, in our case temperature. Levin showed that if one introduces a harmonic perturbation of the system (i.e. a test force) $F_0 \cos \omega t f(\vec{r})$, then the admittance corresponding to that force can be written in terms of the power dissipation in the following manner:

$$|Re[Y(\omega)]| = \frac{2W_{diss}}{F_0^2}, \tag{2.10}$$

with the full derivation appearing on page 660 of [15]. This means:

$$S_x = \frac{2k_B T}{\pi \omega^2} \frac{W_{diss}}{F_0^2}. \tag{2.11}$$

So in order to find an expression for $S_{\delta T}$, we can do the following: apply a "test force" to our fiber system, calculate the expressions for W_{diss} and F_0 given that test force, and finally substitute into equation (2.11) to get the PSD for temperature fluctuations.

There are a few subtleties, however. First of all, we need to understand what exactly

is a force when it comes to temperature fluctuations. For the case of the LIGO test mass, the fluctuations were those of the position of the mirror, and consequently a test force in the traditional sense made much sense. F and x formed a generalized force-coordinate pair, with $W = Fx$. For temperature, however, we need to think of a different generalized force: namely, entropy. Variations in entropy are related to variations in heat according to $Q = Tds$, useful in the equations for thermal conduction. It might seem strange to think of an "entropic" force in this sense. After all, the idea of applying a test force - or even pressure - on a mirror is an intuitive one, whereas it is difficult to even conceptualize what an entropy force even looks like physically. For now, it suffices to remark that entropy is the state function corresponding to temperature. The exact form of the external perturbation does not matter, so much as the response of temperature to that perturbation. In case of the LIGO test mirrors, force too remained abstract as an external perturbation without necessarily being attached to any "physical" mechanism. We need not be concerned with what caused the "force on the mirror" or the "perturbation in entropy," because the physics we are interested in is less in the exact nature of the perturbation, so much as the response of the system to the perturbation. To arrive at an understanding of this response, we run thought experiments: applying imaginary "forces" which take the form of $F_0 \cos \omega t f(\vec{r})$, and then calculating the corresponding dissipation. Once completed, we can vary ω to arrive at an understanding of the response/dissipation of a system for different frequencies.

Let's go through this process for the case of temperature fluctuations in fiber. Because the local fluctuations are sampled using a Gaussian beam, our formula for the entropy force will need to have a form factor matching that of the laser beam profile. Writing the cosine term as an exponent and normalizing, this gets us:

$$\delta S(r,t) = \frac{F_0}{\pi r_0^2 l} e^{-r^2/r_0^2} e^{-i\omega t}, \tag{2.12}$$

where r_0 is the effective radius of the Gaussian power profile and l is the fiber length.

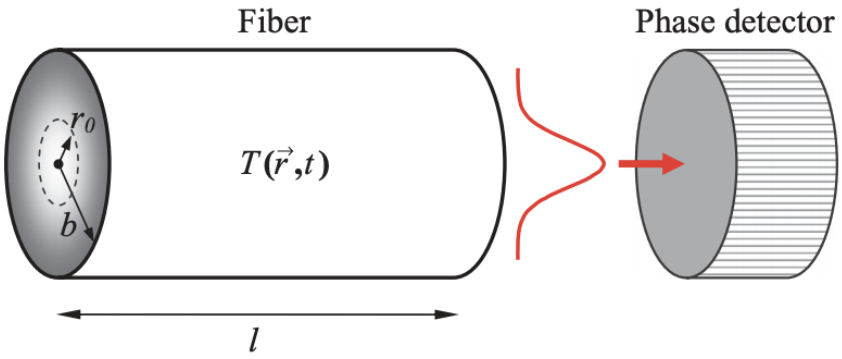

Figure 2.1: Gaussian beam profile of light propagating in fiber [6]

It was difficult to express this perturbation in terms of temperature, because temperature itself is complexly varying parameter which given as the solution of a differential equation according to the general theory of thermal conduction. An entropy change, however, gives rise to a heat change according to $Q = T\Delta S$, which can be inserted into the differential equation for conduction as follows:

$$\kappa \ {}^2\delta T - C_v \frac{\partial \delta T}{\partial t} = T \frac{\partial \delta S}{\partial t}, \tag{2.13}$$

which, along with the time derivative, represents the change in energy over time. Here, κ is the thermal conductivity and C_V is the volumetric heat capacity. Plugging in our expression for the entropic force from equation (2.12) and breaking up the operator into the components of r, we get:

$$\frac{\partial^2 \delta T}{\partial r^2} + \frac{1}{r}\frac{\partial \delta T}{\partial r} - \frac{1}{D}\frac{\partial \delta \partial T}{\partial t} = \frac{-i\omega F_0 T}{8\pi l \kappa} e^{-r^2/r_0^2} e^{-i\omega t}. \tag{2.14}$$

The solution to equation (2.14) can be found in equation (11) of Wanser [21]. From the right hand side of the differential equation, it is clear that the system will have some element of *dissipation*. Wanser derives an expression for this as well:

$$W_{diss} = \frac{\omega^2 F_0^2 T}{8\pi l \kappa} Re[e^{2i\psi_0} E_1(2i\psi_0)] \tag{2.15}$$

where $\psi_0 = \dfrac{\omega r_0^2}{4D}$, $E_1(x)$ is the special function of the exponential integral, and $D = \dfrac{\kappa}{C_V}$. For the sake of completeness, the function for $E_1(x)$ is given as:

$$E_1(x) = \int_x^\infty \frac{e^{-t}}{t} dt. \tag{2.16}$$

We now have the ingredients to calculate the PSD for thermal noise according to equation (2.11). Plugging in our expression for W_{diss}:

$$S_{\delta T}(\omega) = \frac{k_B T^2}{4\pi^2 l \kappa} Re[e^{\frac{i\omega r_0^2}{2D}} E_1(e^{\frac{i\omega r_0^2}{2D}})]. \tag{2.17}$$

This is the full expression of the PSD for temperature fluctuations. However, in practice, calculating E_1 at each ω can be quite tedious. To subvert this, in practice we will use an approximation for equation (2.17) derived by Wanser, valid in the case where $\dfrac{\omega}{v}$ is negligible, v being the velocity of light in the fiber:

$$S_{\delta T} = \frac{k_B T}{4\pi^2 l \kappa} \ln \left[\frac{k_{max}^4 + \frac{\omega^2}{D^2}}{k_{min}^4 + \frac{\omega^2}{D^2}} \right]. \tag{2.18}$$

Here, D is the thermal diffusivity, $k_{max} = 2/w_0$ (w_0 being the fiber mode-field radius), and $k_{min} = 2.405/a_f$ (a_f being the fiber outer diameter). A comprehensive table of the constants and the values used can be found in the Appendix. The presentation here differs from the usual development of Wanser's formula only in that we have kept the terms corresponding to S_T and S_ϕ separate for clarity. A simple substitution is all that is needed to get a final expression for S_ϕ.

Finally, looking towards a calculation for stain, we need convert our PSD into root mean squared (rms) fluctuations in phase noise:

$$\frac{\phi_{rms}(l,\omega)}{\sqrt{Hz}} = \sqrt{4\pi S_\phi(L,\omega)}. \tag{2.19}$$

This follows the form given in Bartolo [2]. We now have a general expression for the thermoconductive phase noise of our system at a given frequency.

2.3 Thermomechanical Noise

Thermoconductive effects arise from random fluctuations of the fiber length or index of refraction due to temperature. Thermomechanical effects, by contrast, are caused by the internal friction – or structural damping – of the medium. While the overall picture of such internal friction is unclear, it can be thought of as related to Brownian motion, where the random motion of the glass particles induce phase changes on the propagating laser light.

The effects of this mechanical damping can be understood using the normal mode expansion [6]. We treat each normal mode as a harmonic oscillator, which has admittance:

$$Y_x(\omega) = \frac{\omega k\phi(\omega) + i(\omega k - m\omega^3)}{(k - m\omega^2)^2 + k^2\phi^2(\omega)} \tag{2.20}$$

Substituting into the FDT, the PSD for each mode i then goes as (remember, the FDT takes only the real part of Y_x):

$$S_{L,i}(\omega) = \frac{k_B T}{\pi\omega} \sum_i \frac{\omega_i \phi_i(\omega)}{m_i[(\omega^2 - \omega_i^2)^2 + \omega_i^4 \phi_i^2(\omega)]} \tag{2.21}$$

where m_i, ω_i, and $\phi_i(\omega)$ are the mass, normal mode frequency, and loss angle associated with each mode i. To solve for ω_i for a single mode, it is reasonable to approximate the fiber as a thin rod in one dimension, and so to use the one dimensional elastic wave equation:

$$\frac{\partial^2 u_z}{\partial z^2} - \frac{\rho}{E_0}\frac{\partial^2 u_z}{\partial t^2} = 0 \tag{2.22}$$

where ρ is the density and E_0 the Young's modulus. Solving this equation yields:

$$u_{z,N}(z,t) = w_n(z)e^{-i\omega_n t} \tag{2.23}$$

where $\omega_N = \frac{n\pi}{l}\sqrt{\frac{E_0}{\rho}}$. From this the effective mass for each mode i can be shown to be: $m_N = \frac{\rho A l}{2}$. Substituting into equation (2.21), and assuming that the loss angle is frequency independent and constant across modes:

$$S_{L,i}(\omega) = \frac{2k_B T l \phi_0}{\pi^3 A E_0 \omega} \sum_i \frac{1}{i^2[(1 - \frac{\omega^2}{\omega_i^2})^2]} \tag{2.24}$$

For high frequencies, this expression need be solved numerically, summing over the modes i (summing up to $N = 10$ is normally reasonable as the higher orders make only minor contributions to power). However when the frequency ω is much less than the frequency of the first mode ω_1, the frequency terms vanish, and we can easily take the sum over i of $\frac{1}{i^2}$ to be $\frac{\pi^2}{6}$. This gives:

$$S_L(\omega) = \frac{k_B T l \phi_0}{3\pi A E_0} \frac{1}{\omega} \tag{2.25}$$

ϕ_0 is the loss angle, A the cross-sectional area of the fiber, and E_0 the bulk modulus. Once again, we are interested in the rms fluctuations of the phase noise:

$$\frac{\phi_{rms}(l,\omega)}{\sqrt{Hz}} = \frac{2\pi}{\lambda}\sqrt{S_L(\omega)} \tag{2.26}$$

Similar to the derivation for thermoconductive noise above, we now have an expression for thermomechanical phase noise as a function of frequency.

There are a few things to remark on. First, is the $1/f$ dependence of the PSD, a familiar form for thermal noise sources of this kind. Second, is the significance of the loss angle for the magnitude of the thermomechanical noise. The Young's modulus E_0 of the material, the cross sectional area A, and Boltzmann's constant are relatively fixed parameters when compared to T, l, and ϕ_0. While optimizing these three para-

meters represents that most straightforward road for improving thermomechanical noise, in general implementing advanced cooling systems and increasing the length of the fiber tend to be hard, as will be discussed further in Chapter 5. Consequently, engineering the material properties so as to lower loss angle is of great significance. Depending on the value of this loss angle, thermomechanical noise can either be more or less punishing than the thermoconductive noise sources derived above. In our final noise analysis of thermomechanical noise in Chapter 5, we will thus take both optimistic and pessimistic approaches in order to arrive at a fuller picture of the loss angle's potential impact. For now, though, we move on from the linear noise sources treated in this chapter to nonlinear scattering effects, which have important consequences for maximum input laser power and overall device sensitivity.

Chapter 3

Scattering Noise Sources

The thermal fluctuations treated in the previous chapter are a source of linear noise in fibers and essentially do not scale with the laser power. In that sense, they are intrinsic sources of uncertainty which arise due to the material and elastic properties of the fiber itself, rather than the specific nonlinear response of the fiber to a driving laser field. Here, we turn our attention to scattering sources. Specifically, Stimulated Brillouin and Raman Scattering. We will see that counter to their thermal noise counterparts, scattering effects do in fact scale with input power, and so have significant consequences for our ability to circumvent limits from one of the most restricting sources of error in high-precision systems – quantum shot noise.

3.1 Stimulated Brillouin Scattering

Stimulated Brillouin scattering (SBS) is a third order, nonlinear process which occurs when a forward propagating photon transforms into a photon at lower energy and an acoustic *phonon*. This occurs due to electrostriction: the passing of an electric field displaces the ions in the dielectric material in different directions based on the signs of the charges, warping the shape and creating a net strain. This induces the phonons. Since the generated phonon typically moves in the forward direction, the scattered photon at lower energy typically moves in the backward direction in order to conserve momentum.

Figure 3.1 depicts the conversion of forward-propagating photons to the scattered

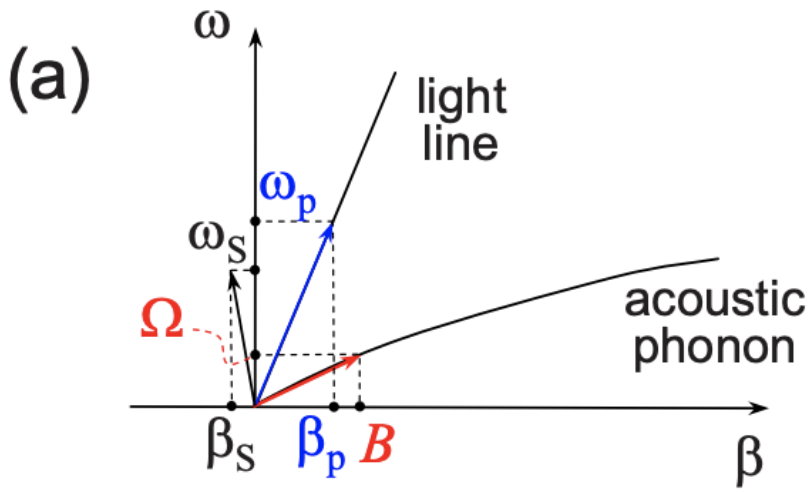

Figure 3.1: Dispersion diagram showcasing the input and output momenta/energy of the particles involved in SBS [13]

particles in the form a dispersion plot. During the process, both energy (symbolized by frequency on the y axis, ω) and momentum (denoted by β on the x axis) must be conserved. The "light line" represents the pump photon and is indexed by p with energy ω_p and momentum β_p. The scattered photon is indexed by s, while the acoustic phonon is taken to have (Ω,B) for its energy/momentum. As expected, the two light sources follow linear dispersion relations. The dispersion relation for the acoustic phonon can be approximated to be linear for small β.

For SBS, then, the most important parameter is the percentage of input optical power which is converted into backward-propagating light. As this input power increases, the processes which drive electrostriction increase as well, reaching a point where the *entire* input power is lost to scattering. In order to mitigate such scattering and to allow for propagation at all, it will be necessary to set limits on the laser input power. Calculating the percentage of scattered light is an important task for determining such a limit, which is what we do next.

3.1.1 Solution for the Density Variation and Power Threshold

The scattered waves from SBS have two components: the backward-propagating optical photons and the forward-propagating acoustic phonons. In this section, we go

through the mathematics for the acoustic phonons, which manifest as a perturbation in the material density of the fiber.

We begin with the differential equation for material density, following the derivation presented in Kobyakov et al. [13], and including terms for damping, sound, and electrostriction:

$$\frac{\partial^2 \rho}{\partial t^2} - \Gamma \quad ^2 \frac{\partial \rho}{\partial t} - v_A^2(r) \quad ^2 \rho = \frac{\gamma_e}{2} \quad ^2 E^2 \tag{3.1}$$

where ρ is the density fluctuation around the mean value ρ_0, Γ is the damping factor, v_A is the squared longitudinal sound velocity, and γ_e is the electrostriction constant.

As implied by the expression, the differential equation prescribes how the material density changes when some external field is applied to the system. In our case, it links the applied laser field to the consequent change in density, i.e. the phonon induced by Brillouin scattering. Our expression for the electric field is a superposition of forward- and backward-propagating waves, according to the two halves of the Brillouin process:

$$\vec{E}(r,z,t) = \frac{1}{2}[A_1(z,t)e^{i(\omega_1 t - \beta_1 z)}\vec{u_1} + A_2(z,t)e^{i(\omega_2 t - \beta_2 z)}\vec{u_2}] + c.c. \tag{3.2}$$

where $f(r)$ is the laser mode profile (i.e. Gaussian) and $A_j(z,t)$ are the slowly varying envelopes of the field.

Taking the gradient of equation (3.2) yields:

$$^2 E^2 = -\frac{1}{2} f^2(r) A_1(z,t) A_2(z,t) \beta_s^2 e^{i(\Omega_d - \beta_s z)} + c.c. \tag{3.3}$$

where $\Omega_d = \omega_1 - \omega_2$ and $\beta_s = \beta_1 + \beta_2$. Substituting equation (3.2) into (3.1) gives us a differential equation which can be solved by guessing solutions of the form:

$$\rho(z,t,r) = \frac{1}{2}[\sum_{m=1}^{M} \bar{\rho}_m(z,t)\xi_m e^{i(\Omega t - qz)}] + c.c. \tag{3.4}$$

Here, the sum is over all the acoustic modes of the fiber, Ω is the frequency of the acoustic wave, and q is the wave vector for the density variation. To make this equation intuitive, notice than within the sum we simply have the product of a plane wave ($e^{i(\Omega t - qz)}$, the mode profile (ξ_m), and the amplitude of the density variation (ρ_m)

One can plug equation (3.3) into the differential equation and solve for $\bar{\rho}_m$ in order to get a final expression for the density variation. Because the math involved is substantial, we simply quote the final result

$$\rho(z,t,r) = \frac{1}{4}\sum_{m=1}^{M}[\xi_m(r)\frac{\xi_m(r)f^2(r)}{\xi_m^2(r)}\frac{\gamma_e q^2 A_1(z,t)A_2(z,t)}{\Omega_m^2 - \Omega^2 + i\Omega\Gamma q^2}e^{i(\Omega t - qz)}] + c.c. \tag{3.5}$$

The expression showcases the decomposition of the phononic modes into forward (the summation) and backward (the complex conjugate) propogating waves. The terms can be thought of as follows: $\frac{\xi_m(r)f^2(r)}{\xi_m^2(r)}$ represents the overlap of the phononic mode and laser profile, and so indicates the coupling between the two. The frequency dependent term represents the response of the system versus frequency, and follows a similar form to the response of a driven harmonic oscillator. Finally, the exponent represents a plane wave.

From the differential equations and solution above, one can switch back to the optical modes and backtrack to get an expression for the optical power threshold. This represents the power at which the magnitude of the scattered beam at the output becomes greater than that of the original forward propogating beam beam at output:

$$P_{th} = \frac{21bA_{eff}}{g_B L_{eff}} \tag{3.6}$$

where A_{eff} is the core area of the fiber, L_{eff} is the effective length, and g_B is the Brillouin gain.

In Chapter 4, we will see how the power threshold dictated by Equation 3.6 will come to set a limitation on overall input and so on quantum shot noise.

3.2 Stimulated Raman Scattering

The nonlinear effects we dealt with in the preceding section on Stimulated Brillouin Scattering arose from the processes of electrostriction, the stretching and squeezing of a material due to an applied electric field. In this section we briefly examine Stimulated Raman Scattering (SRS) - another scattering process which arises instead by excitations and de-excitations of the vibrational modes of molecules in the material itself. These excitations can induce propogating *optical phonons* in the fiber material, as opposed to the acoustic phonons we saw for SBS. Another important difference is that because of the excitation mechanism, scattered waves in SRS can propagate either forward or backwards, and can even showcase gain. This property has even been used to create SRS-based amplifiers.

Analyses of SRS proceed in a very similar manner to those of SBS: with the differential equations coupling pump, phononic, forward-propogating, and backward-propogating waves being used to arrive at an overall power threshold - representing the input power at which the magnitude of the scattered wave at the output becomes equivalent to the pump wave also at the output. Carrying out these calculations, it turns out that the magnitude of the scattered waves for SRS are much smaller (more than two orders of magnitude) than those for SBS, with a power threshold at around 450 mW as compared to the 30 mW threshold found for SBS [18]. Because of this, for the final noise analysis in the next chapter, we assume that any power low enough to mitigate SBS will also suffice for suppressing the effects of SRS.

Having understood the limitations on power caused by stimulated scattering effects, we now move on to conduct a final noise analysis of the sensitivity limits of an optical fiber interferometer.

Chapter 4

Results

Having derived analytic expressions for thermal noise and Brillouin scattering, we now carry out the final noise analysis by entering those noise models into the software package Gravitational Wave Interferometer Noise Code (GWINC) [11]

The different noise contributions for a hypothetical fiber-based Michelson interferometer are shown in the figures below.

4.1 Thermal Noise

Fig 4.1 shows the strain sensitivity curves for the Wanser and Duan models at room temperature, corresponding to thermoconductive and thermomechanical noise respectively. The Wanser model, shown in red, holds flat at a strain of about $10^{-16}/\sqrt{Hz}$ until a frequency of about 3 kHz. Conversely, the strain sensitivity curve of the Duan model descends inversely proportional to $\sqrt{\omega}$, with the blue and green curves evaluated at mechanical loss angles of 10^{-2} and 10^{-5}, respectively.

The rms phase noise expressions derived in the preceding chapters need to be converted into the units of strain sensitivity. We divide by the total amount of radians in an interferometer of length l:

$$strain = \frac{\frac{\phi_{rms}(l,\omega)}{\sqrt{Hz}}}{0.78\phi_{rad}(l)} = \frac{\frac{\phi_{rms}(l,\omega)}{\sqrt{Hz}}}{l \times 5.421 \times 10^6} \tag{4.1}$$

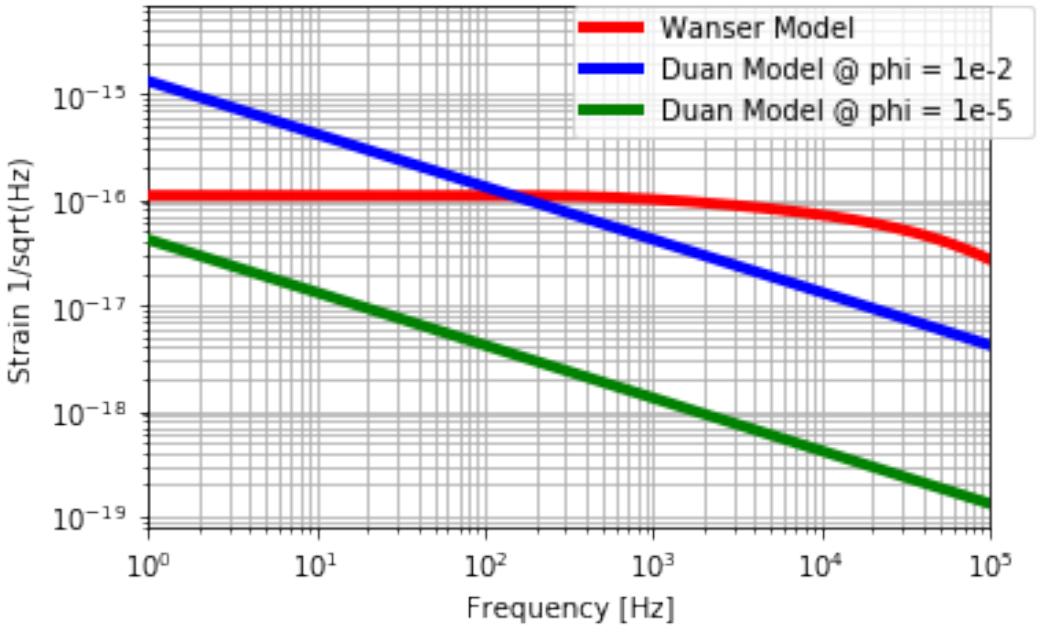

Figure 4.1: Thermomechanical (blue, green), and thermoconductive (red) noise curves for an interferometer arm length of 10 km at room temperature.

where we have taken $l = 10$ km for the calculations below, in line with the interferometer arm length of Advanced LIGO.

We plot the Duan model at two different loss angles, one more pessimistic (blue), the other optimistic (green).

The limits on sensitivity set by thermal noise are significant. The Wanser model alone sets a noise floor of around $10^{-16}/\sqrt{Hz}$ at frequencies below 3 kHz, between six and seven orders of magnitude higher than the current strain sensitivity of Advanced LIGO in the same frequency range. In principle, the thermoconductive effects captured by the Wanser model can be mitigated by engineering the thermal expansion and refractive effects to cancel with each other (in Equation 2.8, this would take the form of a negative expansion coefficient), however, tuning the parameters in this way comes with the possible trade off of a higher loss angle in the Duan model.

Cooling can also lead to a lower noise floor. But while temperatures lower than room temperature are in principle achievable, it would be extremely difficult for cooling alone to make up the gap. For example, given the $\sqrt{T}$ dependence of the strain

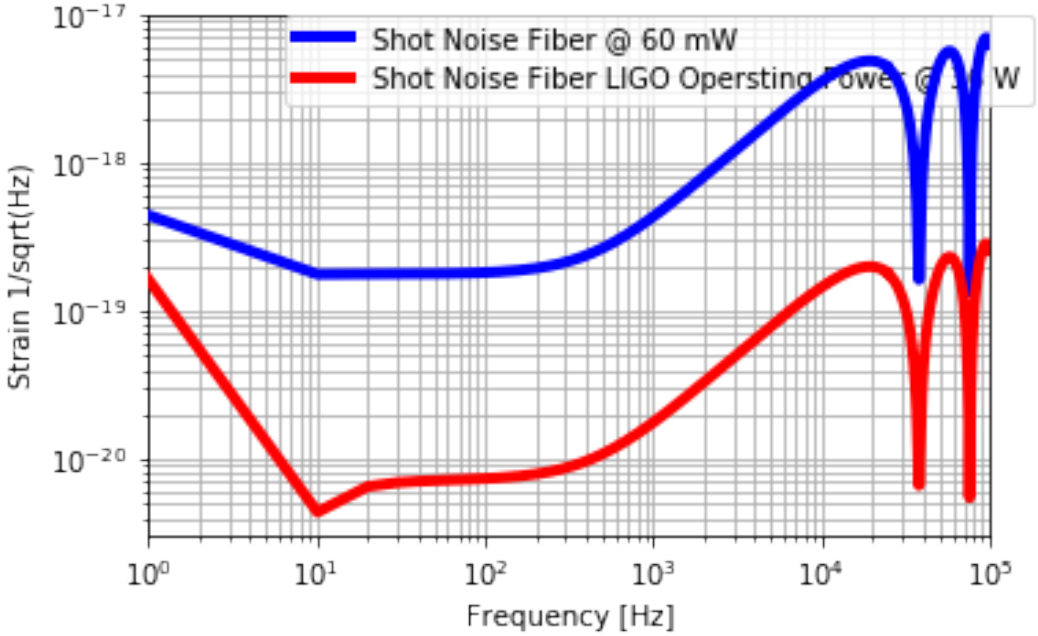

Figure 4.2: Shot noise comparison between 60 mW light beam propagating in fiber (blue) and Advanced LIGO operational power of about 33 W (red). Power level in fiber set to minimize SBS and SRS effects.

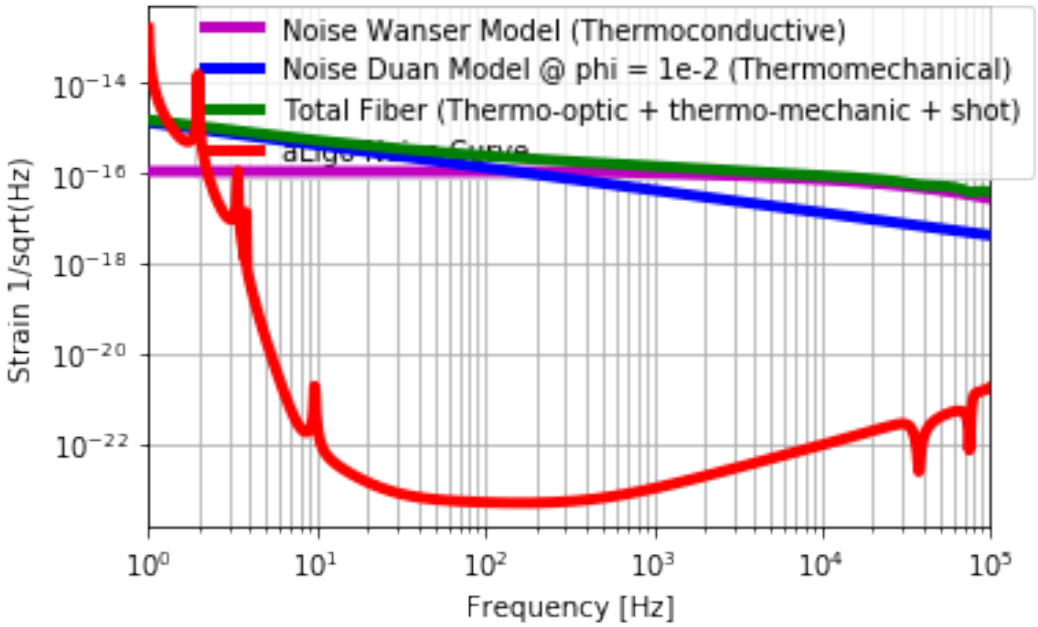

Figure 4.3: Strain sensitivity of total thermal-optic (purple) and thermo-mechanical (blue) noise sources in fiber plotted in reference to the Advanced LIGO sensitivity curve

sensitivity and the change in material constants due to changes in temperature, bringing the fiber spool down to the temperature of liquid helium would lead to an improvement of an order of magnitude at best. Alternative cooling schemes exist in the literature, but by and large they operate between 80 K and room temperature [23], and it is not clear whether such procedures could be applied to the presumably much larger space required to house a fiber coil with a length upwards of 10 km. The few schemes which do use dilution refrigerators to achieve temperatures in the hundreds of milliKelvin operate in incredibly restricted spaces and consequently it appears all the more difficult to apply them to a hypothetical fiber interferometer [23, 12].

The final option for thermal noise mitigation is to search for alternative fiber platforms than the Silica-based fibers used here (see Section 4.1).

4.2 Shot Noise

Fig 4.2 depicts the total thermal noise together with the shot noise and Brownian noise curves as reference. The strain sensitivity for shot noise scales inversely with the square root of laser power. Laser power, however, is limited by the scattering noise sources mentioned in the introduction. Because Stimulated Brillouin Scattering (SBS) and Stimulated Raman Scattering (SRS) scale with laser power, here the laser power was kept low enough to suppress their presence. An input power of 60 mW was used for the calculations of shot noise.

When fibers were first considered as a platform for gravitational wave detection in the late 1980's, the restrictions set on shot noise sensitivity by SBS and SRS were a fundamental concern that appeared to set a stringent limit on the ultimate strain sensitivity of a fiber interferometer [16]. However, two developments since then have led to progress in this area. Improvements in fiber attenuation, which captures the proportion of laser power retained in fibers given travel over some distance and is an important factor for determining the magnitude of scattering effects, mean that higher laser powers overall can be maintained before SBS and/or SRS begin to

dominate. Additionally, the perfection of squeezing as a technique offers the potential to further lower the shot noise floor with lower laser power.

4.3 Brownian Noise and Fiber Amplifiers

Like shot noise, Brownian noise related to the test mass suspension system is important to the make up of the Advanced LIGO sensitivity curve. It is also an area where a fiber detector could stand to make gains on a free beam setup.

It is not clear whether a fiber interferometer would need to utilize suspended test masses at all. In principle, coated mirror ends appended directly on to the fiber could serve to reflect the light beam, saving on the loss introduced in using silica glass fibers for suspension. The gain in sensitivity made possible by such a switch is still an open question. Nevertheless, the issue of Brownian noise caused by suspension present a domain where fiber technology may have an advantage.

The noise curves above leave out one important factor: the inevitable need for fiber amplifiers. At 1060 nm, the state of the art for the attenuation in Silica fibers stands at 0.57 dB/km, meaning a large fraction of laser power is lost during transmission over large distances. Fiber amplifiers can be used to recuperate the power loss, but with the price of introducing excess noise into the system. Standard optical fiber amplifiers are quoted with noise figures of 3 dB [4], corresponding to an increase of the PSD for thermal noise by about a factor of 1.3 per amplifier. It is important to note that strain sensitivity scales with the square root of the thermal noise PSD. Nevertheless, the excess noise introduced by fiber amplifiers is another significant hurdle in achieving the requisite sensitivity level. There is extensive literature detailing the additional noise sources introduced by fiber amplifiers, as well as proposed schemes for mitigating such excess noise. These will be the subject of future study in the context of fiber-based GW detectors.

Chapter 5

Conclusion and Future Directions

An optical fiber interferometer for detecting gravitational waves is an exciting prospect. In the preceding chapters we have established that a fundamental hurdle for realizing such a scheme is unmanageable thermooptic and thermomechanical phase noise effects in fibers.

With current Silica-based platforms, the strain sensitivity of a fiber-based Michelson interferometer operating at room temperature and with 10 km arm lengths is limited to $10^{-16}/\sqrt{Hz}$ at 100 Hz, nearly seven orders of magnitude higher than the comparable operating sensitivity of Advanced LIGO. This sensitivity is almost completely set by thermal noise sources, but is an underestimate due to excess noise introduced by fiber amplifiers which are necessary to combat power loss.

Given the stringent limit set on strain sensitivity in Silca-based fibers, one might ask if there are other potential fiber platforms which might showcase improved noise profiles. For example, the class of relatively new fiber technologies which includes photonic crystal (PC) and hollow core (HC) platforms have already demonstrated potential when it comes to applications as diverse as data transfer using 5G, the synchronization of financial transactions, and communication between networks of widely spaced telescopes [20]. Do these advantages apply as well to the problem of mitigating thermal noise and using a fiber interferometer for gravitational wave detection?

The properties of PC/HC platforms are well documented when it comes to meas-

urements of the thermal coefficient of delay (TCD) constant - the parameter most important for the applications mentioned above. But comprehensive characterizations of thermal phase noise in these new fiber platforms have yet to occur. Early studies have yet to show any advantage for PC/HC [17, 19], but this comparison is skewed, as not as much attention has been given to parameter optimization and noise mitigation in these novel platforms.

Advantages have been demonstrated when it comes to the less restrictive issue of the scattering noise sources, however. In particular, reductions of Stimulated Brillouin Scattering of up to one to two orders of magnitude have been noted, potentially paving the way for higher operating powers and lower shot noise floors in fibers [5]. In general, however, the full ramifications of HC/PC fibers for strain sensitivity in high precision fiber interferometers are not yet well understood and represent an active area of investigation.

When fiber technology was assessed for gravitational wave detection in the late 1980s, Standard Brillouin and Raman scattering seemed to set a fundamental limit on the shot noise sensitivity of fiber interferometers. Improvements since then in fiber attenuation constants and squeezing techniques may indicate progress in this area.

The avenues for improving thermal noise in optical fibers mentioned above represent directions for technological development. The question of mitigating thermal noise – and so of detecting gravitational waves in an optical fiber interferometer – remains an area of active investigation and research. Though it must be noted that a sizable advancement would be needed in order to overcome the factor of a million difference between the strain sensitivity of Advanced LIGO and a hypothetical fiber interferometer [1].

References

[1] B. P. Abbott et al. 'Observation of Gravitational Waves from a Binary Black Hole Merger'. In: *Phys. Rev. Lett.* 116 (6 Feb. 2016), p. 061102. DOI: 10.1103/PhysRevLett.116.061102. URL: https://link.aps.org/doi/10.1103/PhysRevLett.116.061102 (cit. on pp. 1, 2, 36).

[2] R. E. Bartolo, A. B. Tveten and A. Dandridge. 'Thermal Phase Noise Measurements in Optical Fiber Interferometers'. In: *IEEE Journal of Quantum Electronics* 48.5 (2012), pp. 720–727. DOI: 10.1109/JQE.2012.2190717 (cit. on pp. 11, 22).

[3] Herbert B Callen and Theodore A Welton. 'Irreversibility and generalized noise'. In: *Physical Review* 83.1 (1951), p. 34 (cit. on pp. 11, 12).

[4] Carlton M. Caves. 'Quantum limits on noise in linear amplifiers'. In: *Phys. Rev. D* 26 (8 Oct. 1982), pp. 1817–1839. DOI: 10.1103/PhysRevD.26.1817. URL: https://link.aps.org/doi/10.1103/PhysRevD.26.1817 (cit. on p. 34).

[5] Paulo Dainese et al. 'Stimulated Brillouin scattering from multi-GHz-guided acoustic phonons in nanostructured photonic crystal fibres'. In: *Nature Physics* 2 (May 2006), pp. 388–392. DOI: 10.1038/nphys315 (cit. on p. 36).

[6] Lingze Duan. 'General treatment of the thermal noises in optical fibers'. In: *Phys. Rev. A* 86 (2 Aug. 2012), p. 023817. DOI: 10.1103/PhysRevA.86.023817. URL: https://link.aps.org/doi/10.1103/PhysRevA.86.023817 (cit. on pp. 11, 20, 22).

[7] Sheila Dwyer et al. 'Gravitational wave detector with cosmological reach'. In: *Physical Review D* 91.8 (Apr. 2015). ISSN: 1550-2368. DOI: 10.1103/physrevd.91.082001. URL: http://dx.doi.org/10.1103/PhysRevD.91.082001 (cit. on p. 7).

[8] *Fabry-Perot Cavity*. URL: https://www.teachspin.com/fabry-perot (cit. on p. 7).

[9] FAVPNG.com. *Virgo Interferometer LIGO Michelson Interferometer Interferometry Fabry–Pérot Interferometer - PNG - Download Free*. URL: https://favpng.com/png_view/light-virgo-interferometer-ligo-michelson-

interferometer-interferometry-fabry-p%C3%A9rot-interferometer-png/qv0WesTN (cit. on p. 5).

[10] Scott Foster, Alexei Tikhomirov and Mark Milnes. 'Fundamental Thermal Noise in Distributed Feedback Fiber Lasers'. In: *IEEE Journal of Quantum Electronics* 43.5 (2007), pp. 378–384. DOI: 10.1109/JQE.2007.894744 (cit. on p. 17).

[11] *gwinc / pygwinc*. URL: https://git.ligo.org/gwinc/pygwinc (cit. on p. 30).

[12] Daisuke Hashimoto and Kaoru Shimizu. 'Cooling an optical fiber to 4.5 K by indirect thermal contact with a liquid-helium flow and spectroscopic temperature measurements'. In: *The Review of scientific instruments* 79 (Oct. 2008), p. 093102. DOI: 10.1063/1.2976681 (cit. on p. 33).

[13] Andrey Kobyakov, Michael Sauer and Dipak Chowdhury. 'Stimulated Brillouin scattering in optical fibers'. In: *Adv. Opt. Photon.* 2.1 (Mar. 2010), pp. 1–59. DOI: 10.1364/AOP.2.000001. URL: http://aop.osa.org/abstract.cfm?URI=aop-2-1-1 (cit. on pp. 26, 27).

[14] R Kubo. 'The fluctuation-dissipation theorem'. In: *Reports on Progress in Physics* 29.1 (Jan. 1966), pp. 255–284. DOI: 10.1088/0034-4885/29/1/306. URL: https://doi.org/10.1088/0034-4885/29/1/306 (cit. on pp. 12, 14).

[15] Yu. Levin. 'Internal thermal noise in the LIGO test masses: A direct approach'. In: *Phys. Rev. D* 57 (2 Jan. 1998), pp. 659–663. DOI: 10.1103/PhysRevD.57.659. URL: https://link.aps.org/doi/10.1103/PhysRevD.57.659 (cit. on p. 18).

[16] Paul Linsay, Peter Saulson and Rai Weiss. 'A Study of a Long Baseline Gravitational Wave Antenna System'. In: (1983) (cit. on pp. 3, 33).

[17] Seth Meiselman and Geoffrey A. Cranch. 'Optical phase response to temperature in a hollow-core photonic crystal fiber'. In: *Opt. Express* 25.22 (Oct. 2017), pp. 27581–27594. DOI: 10.1364/OE.25.027581. URL: http://www.opticsexpress.org/abstract.cfm?URI=oe-25-22-27581 (cit. on p. 36).

[18] Sunil Singh, Ramgopal Gangwar and Nar Singh. 'Nonlinear scattering effects in optical fibers'. In: *Progress in Electromagnetics Research-pier - PROG ELECTROMAGN RES* 74 (Jan. 2007), pp. 379–405. DOI: 10.2528/PIER07051102 (cit. on p. 29).

[19] R. Slavík et al. 'Ultralow Thermal Sensitivity of Phase and Propagation Delay in Hollow-Core Fibres'. In: *2017 European Conference on Optical Communication (ECOC)*. 2017, pp. 1–3. DOI: 10.1109/ECOC.2017.8346100 (cit. on p. 36).

[20] W. Urbanczyk et al. 'Photonic crystal fibers for sensing applications'. In: *2008 IEEE/LEOS Winter Topical Meeting Series*. 2008, pp. 196–197. DOI: 10.1109/LEOSWT.2008.4444468 (cit. on p. 35).

[21] Keith H. Wanser, Alan D. Kersey and Anthony Dandridge. 'Intrinsic Thermal Phase Noise Limit in Optical Fiber Interferometers'. In: *Opt. Photon. News* 4.12 (Dec. 1993), pp. 37–38. DOI: 10.1364/OPN.4.12.000037. URL: http://www.osa-opn.org/abstract.cfm?URI=opn-4-12-37 (cit. on pp. 11, 20).

[22] *Wave interference*. Feb. 2021. URL: https://en.wikipedia.org/wiki/Wave_interference (cit. on p. 6).

[23] Hai Zhong et al. 'A millikelvin all-fiber cavity optomechanical apparatus for merging with ultra-cold atoms in a hybrid quantum system'. In: *Review of Scientific Instruments* 88 (Feb. 2017), p. 023115. DOI: 10.1063/1.4976497 (cit. on p. 33).